JOURNAL OF GUIDANCE, CONTROL, AND DYNAMICS
Vol. 15, No. 5, September-October 1992

H^∞ Synthesis Using a Bilinear Pole Shifting Transform

R. Y. Chiang*
Jet Propulsion Laboratory, California Institute of Technology, Pasadena, California 91109
and
M. G. Safonov†
University of Southern California, Los Angeles, California 90089

An H^∞ control law design is presented for a benchmark problem consisting of an undamped pair of spring-coupled masses with a sensor and actuator that are not collocated. This simple mechanical system captures many of the salient features of more complex aircraft and space structure vibration control problems. The H^∞ problem formulation enables the issue of stability robustness in the face of large mass and spring constant variation to be directly addressed. Constraints on closed-loop dominant pole locations and settling time are accommodated via a simple s-plane bilinear transform. The transform parameter can give direct control of closed-loop disturbance settling time and controller open-loop pole-zero locations. A four-state H^∞ minimum phase controller was found to meet the given specifications of each design. Detailed analysis on the tradeoffs of sensor noise vs control energy are also presented.

I. Problem and Specifications

THE benchmark problem proposed by Wie and Bernstein[1] is shown in Fig. 1. This undamped spring-mass system has the following transfer function

$$\frac{z}{u} = \frac{k}{m_1 s^2\{m_2 s^2 + [1 + (m_2/m_1)]k\}} \tag{1}$$

where the masses m_1, m_2, and the spring constant k take the value of 1.0 as nominal, but can be uncertain. In addition, the measurement variable z (picked up by the sensor) is not collocated with the actuator signal u, which introduces extra phase lag into the system and makes it much harder to control. On the other hand, a collocated actuator/sensor system setup is passive and can never be destabilized by feedback.

Table 1 summarizes the specifications of all three designs. Overall, this problem captures many of the challenging robust control issues encountered in aerospace applications such as robustness vs performance tradeoff, control bandwidth vs control energy, noise rejection, etc.

From the classical design point of view (root locus or Bode plot), this plant can be stabilized and its poles can be assigned to a certain area in the s plane via three lead networks (with each contributing about 70–80-deg phase angle around the crossover frequency region). The question is how to find this controller using modern techniques such as H^2 or H^∞.

II. Design Methodology

Figure 2 presents the flowchart of a five-step design procedure:

Step 1: Pull out the uncertainty blocks from the system block diagram to formulate an H^∞ robust control problem.

Step 2: Map the plant from s plane to $\tilde{s}$ plane via the bilinear pole-shifting transform $s = (\tilde{s} + p_1)/[(\tilde{s}/p_2) + 1]$.

Step 3: Compute the H^∞ optimal controller for the transformed plant $\tilde{T}(\tilde{s})$ (i.e., solve $\min_{\tilde{F}(\tilde{s})}\|\tilde{T}(j\tilde{\omega})\|_\infty < 1$).

Step 4: Map the controller $\tilde{F}(\tilde{s})$ back to the s plane via the inverse bilinear pole shifting transform $\tilde{s} = (-s + p_1)/[(\tilde{s}/p_2) - 1]$.

Step 5: Go back to step 1 and iterate the parameter p_1 of the bilinear transform until the design specifications are met.

The following sections elaborate each step.

A. H^∞ Robust Control Problem Formulation

First, an H^∞ optimal control problem is formulated. The uncertainty in k is represented additively as

$$k = 1.25 \pm 0.75\Delta \tag{2}$$

where the size of Δ is bounded by $\|\Delta\|_\infty \le \gamma$. The uncertainty of spring constant Δ is pulled out, as shown in Fig. 3. The disturbances injected into the system at mass 1 and 2 are denoted as $\omega(t)$. The sensor noise is denoted as $v(t)$. For design 2, uncertainty blocks $(\Delta_{M_1}, \Delta_k, \Delta_{M_2})$ will be pulled out from the system block diagram, and no scaling is needed.

Now, an H^∞ small-gain problem is formulated for all three designs:

Find a stabilizing controller $F(s)$ such that

$$\min_{F(s)}\|T_{y_1 u_1}\|_\infty < \frac{1}{\gamma} \tag{3}$$

with $\gamma = 1$ for designs 1 and 3 and with the greatest possible γ for design 2.

In general, this small-gain problem formulation allows one to capture many of the issues occurring in practical control problems including disturbance attenuation, control bandwidth, plant parametric sensitivity, and performance/robustness tradeoffs, etc.

The state-space H^∞ algorithm can become ill conditioned when the plant has $j\omega$-axis poles or zeros. It can lead to an irrational, noncomputable optimal controller with point discontinuities at the offending $j\omega$-axis poles or zeros. This problem has been discussed thoroughly in Ref. 2.

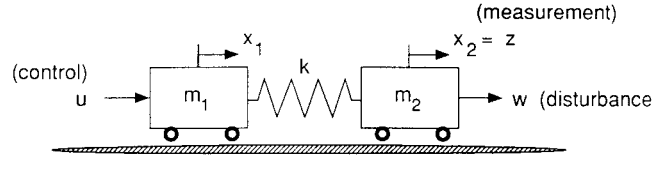

Fig. 1 Benchmark problem.

Received April 10, 1991; revision received Nov. 1, 1991; accepted for publication Nov. 14, 1991.

*Member, Technical Staff.

†Professor, Department of Electrical Engineering.

Table 1 Design specifications

Design	Robustness	Settling time	Disturbance, $w(t)$
1	Stable for $0.5 < k < 2.0$	$T_s \approx 15$ s for nominal	Impulse
2	Maximize MSM[a] of m_1, m_2, k	$T_s \approx 15$ s for nominal	Impulse
3	Stable for $0.5 < k < 2.0$	$T_s \approx 20$ s for nominal	$A \sin(0.5t + \phi)$ A, ϕ unknown

[a]MSM = multivariable stability margin.

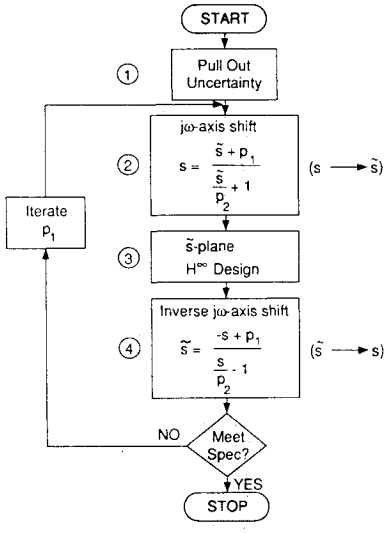

Fig. 2 Design flow chart.

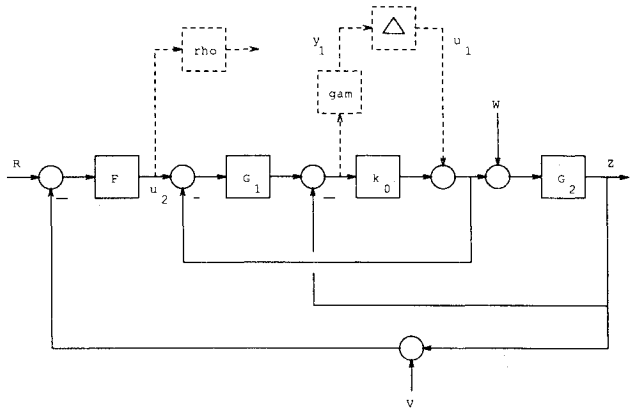

Fig. 3 H^∞ synthesis block diagram.

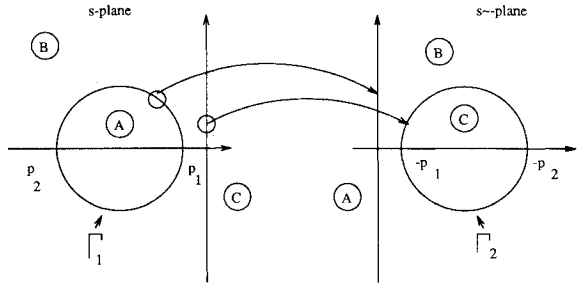

Fig. 4 Bilinear transform on s plane.

B. Bilinear Pole-Shifting Transform ($j\omega$-Axis Shifting)

A simple bilinear transform[2] has been found extremely useful for removing the H^∞ ill-posedness problem and achieving the design specifications for the benchmark problem.

First, the bilinear transform is formulated as $j\omega$-axis pole shifting transformation

$$s = \frac{\tilde{s} + p_1}{(\tilde{s}/p_2) + 1} \tag{4}$$

where the negative numbers p_1 and p_2 are the endpoints of the diameter of a circle in the left s plane (see Fig. 4) that is mapped by Eq. (4) onto the $j\tilde{\omega}$ axis in the $\tilde{s}$ plane. The inverse of such a bilinear transform is

$$\tilde{s} = \frac{-s + p_1}{(s/p_2) - 1} \tag{5}$$

Figure 4 also shows how the various regions designated A, B, and C in $s/\tilde{s}$ planes are transformed by the mappings (4) and (5):

1) The boundary of the s-plane circle Γ is mapped onto $j\tilde{\omega}$ axis in the $\tilde{s}$ plane.

2) The s plane $j\omega$ axis is mapped onto a circle $\tilde{\Gamma}$ in the right $\tilde{s}$ plane, which is an exact mirror image of the s-plane circle Γ.

3) Areas A, B, and C are mapped to their $\tilde{s}$-plane counterparts.

Both forward and inverse multivariable bilinear transforms are special cases of the transform $s = (\alpha z + \delta)/(\gamma z + \beta)$ and can be realized by the state-space formula[2-4]:

$$\left[\begin{array}{c|c} A_b & B_b \\ \hline C_b & D_b \end{array}\right] = \left[\begin{array}{c|c} (\beta A - \delta I)(\alpha I - \gamma A)^{-1} & (\alpha\beta - \gamma\delta)(\alpha I - \gamma A)^{-1}B \\ \hline C(\alpha I - \gamma A)^{-1} & D + \gamma C(\alpha I - \gamma A)^{-1}B \end{array}\right] \tag{6}$$

Other important transforms that map continuous transfer functions to discrete domain such as Tustin, prewarped Tustin, backward/forward rectangular transforms, etc., can also be handled with this state-space formula.[3,4]

C. Optimal H^∞ Controller via Loop-Shifting Concept

The H^∞ control theory concerns the design of a control law of the form

$$u_2(s) = F(s)y_2(s) \tag{7}$$

for a two-port plant

$$\begin{bmatrix} y_1(s) \\ y_2(s) \end{bmatrix} = P(s)\begin{bmatrix} u_1(s) \\ u_2(s) \end{bmatrix} \tag{8}$$

where, in general, y_1, y_2, u_1, and u_2 are vectors. The objective in H^∞ control is to choose $F(s)$ such that the closed-loop transfer function $T_{y_1u_1}$ is bounded as

$$\|T_{y_1u_1}\|_\infty < 1 \tag{9}$$

In the usual formulation, the plant is assumed to have an n-state state-space representation with B, C, D matrices partitioned conformably with (y_1, y_2, u_1, u_2), i.e.,

$$P(s) := \left[\begin{array}{c|c} A & B \\ \hline C & D \end{array}\right] = \left[\begin{array}{c|cc} A & B_1 & B_2 \\ \hline C_1 & D_{11} & D_{12} \\ C_2 & D_{21} & D_{22} \end{array}\right] \tag{10}$$

A solution $F(s)$ for the H^∞ control problem may be found by solving two Riccati equations.[7-9]

The two-Riccati H^∞ controller has been derived via two distinct approaches—game theory in time domain and all-pass embedding in frequency domain. The game theory approach is conceptually abstract but leads to a much simpler derivation. In 1977, Mageirou and Ho[5] solved the full-state feedback case via game theory and others[6] later "rediscovered" it. Subsequently, Doyle et al.[7] extended the full-state feedback result into its observer dual and established a separation principle for H^∞ control [a counterpart of the linear quadratic Gaussian (LQG) separation principle]. A frequency domain derivation for the dynamical output feedback case was initiated by Limebeer et al.[8] using Parrott's all-pass embedding technique and the optimal Hankel norm theorem. Both approaches require a large effort and much algebraic manipulation to handle all but very special cases in which the plant C and D matrices satisfied certain conditions. Safonov et al.[9] developed a loop-shifting technique to simplify the derivations, introduced a descriptor matrix-pencil representation and improved existence conditions. The latter eliminated numerical instabilities that had plagued previous formulations of the H^∞ control theory. A matrix pencil is an s-dependent matrix of the form $As + B$. The generalized eigenvalues of a regular square matrix pencil, denoted $\lambda_i(As + B)$, are the values of $s \in \mathcal{C}$ at which the determinant of the pencil vanishes; numerically robust algorithms exist for computing the generalized eigenvalues and associated eigenspaces.[3]

The benchmark problem was solved via the loop-shifting optimal H^∞ formulas.[9] The main results from Ref. 9 are summarized here without proof.

Theorem 1.[9] Suppose the plant D matrix has the special structure

$$D_{11} = 0 \tag{11a}$$

$$D_{22} = 0 \tag{11b}$$

$$D_{12} = \begin{bmatrix} 0 \\ I \end{bmatrix} \tag{11c}$$

$$D_{21} = [0 \;\; I] \tag{11d}$$

Let the Hamiltonian matrices be described as

$$H_c = \begin{bmatrix} A - B_2 D_{12}^T C_1 & B_1 B_1^T - B_2 B_2^T \\ -\tilde{C}_1^T \tilde{C}_1 & -(A - B_2 D_{12}^T C_1)^T \end{bmatrix} \tag{12}$$

$$H_o = \begin{bmatrix} (A - B_1 D_{21}^T C_2)^T & C_1^T C_1 - C_2^T C_2 \\ -\tilde{B}_1 \tilde{B}_1^T & -(A - B_1 D_{12}^T C_2) \end{bmatrix} \tag{13}$$

where

$$\tilde{C}_1 = (I - D_{12} D_{12}^T) C_1 \tag{14}$$

$$\tilde{B}_1 = B_1 (I - D_{21}^T D_{21}) \tag{15}$$

Then, there exists a stabilizing controller $F(s)$ for which $\|T_{y_1 u_1}\|_\infty < 1$, if and only if the Hamiltonian matrices H_c and H_o have no eigenvalues with zero real part and the following three generalized eigenvalue conditions are satisfied:

$$\max_i Re\{\lambda_i[P_1 s - (AP_1 + B_2 \bar{F})]\} < 0 \tag{16}$$

$$\max_i Re\{\lambda_i[S_1 s - (S_1 A + \bar{G} C_2)]\} < 0 \tag{17}$$

$$\max_i \lambda_i(S_1 P_1 s - S_2 P_2) < 1 \tag{18}$$

where P_1, P_2, S_1, S_2 are any $n \times n$ matrices chosen such that the columns of $[P_1, P_2]^T$ and $[S_1^T, S_2^T]^T$ form bases for the respective eigenspaces of H_c and H_o associated with negative eigenvalues and

$$\bar{F} = -(B_2^T P_2 + D_{12}^T C_1 P_1) \tag{19}$$

$$\bar{G} = -(S_2 C_2^T + S_1 B_1 D_{21}^T) \tag{20}$$

Furthermore, one controller for which $\|T_{y_1 u_1}\|_\infty \leq 1$ is given by

$$F(s) = -\bar{F}(Es - \bar{A})^{-1} \bar{G} \tag{21}$$

where

$$\bar{A} = S_1 \tilde{A} P_1 + S_2 \tilde{A}^T P_2 + S_1(\tilde{B}_1 \tilde{B}_1^T - B_2 B_2^T) P_2 + S_2(\tilde{C}_1^T \tilde{C}_1 - C_2^T C_2) P_1 \tag{22}$$

$$\tilde{A} = A - B_2 D_{12}^T C_1 - B_1 D_{21}^T C_2 \tag{23}$$

$$E = S_1 P_1 - S_2 P_2 \tag{24}$$

The loop-shifting techniques described in Safonov et al.[9] will transform a general plant to the special structure required by Eqs. (11a-d) of Theorem 1. The final controller is assembled via the inverse loop-shifting transforms.[9]

The formulas and existence conditions in Theorem 1 and the loop-shifting transforms[9] have been implemented in the H^∞ software[3] since December 1988. We note that Ref. 9 also includes a result parameterizing all controllers for which $\|T_{y_1 u_1}\|_\infty \leq 1$.

D. Properties of the Optimal H^∞ Controllers

Several interesting and well-known properties of the H^∞ theory are summarized here without proof:

Property 1. The optimal H^∞ cost function $T_{y_1 u_1}$ is all pass, i.e., $\bar{\sigma}[T_{y_1 u_1}(j\omega)] = 1$ for all $\omega \in \mathcal{R}$.

Property 2. In any weighted mixed sensitivity problem formulation (e.g., Safonov and Chiang[13]), the H^∞ controller always cancels the stable poles of the plant with its zeros (transmission zeros).

Property 3. In the weighted mixed sensitivity problem formulation (e.g., Safonov and Chiang[13]), any unstable pole of the plant inside the specified control bandwidth [i.e., the frequency range where the sensitivity weight $W_1(s)$ defined in Ref. 9 satisfies $|W_1(j\omega)| < 1$] will be shifted approximately to its $j\omega$-axis mirror image once the feedback loop is closed with an H^∞ optimal controller.

Property 1 enables the mixed-sensitivity H^∞ to be an exact loop-shaping control design tool.[3] Property 2 unfortunately implies that mixed-sensitivity H^∞ design will inevitably suffer stability robustness problems when there are parametric variations affecting the locations of lightly damped plant poles. (Two methods are proposed in Ref. 10 to improve this deficiency.) Property 3 enables this loop-shifting H^∞ method to work successfully in resolving the latter difficulty as well as the benchmark problem.

Recall the following property of the bilinear mapping: The poles on the $j\omega$ axis in s plane are mapped into a circle $\bar{\Gamma}$ in $\bar{s}$ plane centered at $-(p_1 + p_2)/2$. Property 3 will ensure the closed-loop poles are placed inside the circle A in s plane of Fig. 4 at positions that are the shifted RHP mirror images of the open-loop poles outside the region A in $\bar{s}$ plane. Therefore, the parameter p_1 in bilinear transform plays a significant role of placing the dominant closed-loop poles at the desired locations in s plane, thereby determining noise rejection and settling time, etc. The variable p_1 turns out to be the only parameter that needs to be adjusted for all of the designs to meet the benchmark problem specifications.

E. Smaller H^∞ Norm in s Plane

Another salient feature of the bilinear pole-shifting method is that the maximum modulus theorem guarantees that the

following inequality is satisfied[2]:

$$\|T(j\omega)\|_\infty = \sup_\omega \bar{\sigma}[T(j\omega)] \le \sup_{s\in\Gamma} \bar{\sigma}[T(s)] = \sup_{\tilde{\omega}} \bar{\sigma}[\tilde{T}(j\tilde{\omega})] = \|\tilde{T}(j\tilde{\omega})\|_\infty < 1 \tag{25}$$

Therefore, it ensures that the final s-plane controller $F(s)$ will at least meet the robustness specification ($\|\Delta\|_\infty \le \gamma$) and will probably exceed it.

III. Design Results

The values of design parameters in bilinear transform $s = (p_1 + \tilde{s})/(1 + \tilde{s}/p_2)$ that were used in our design study are summarized in Table 2. The parameter p_1 was selected via a simple rule of thumb in classical control[11]

$$T_{\text{settling}} \approx \frac{4}{\zeta\omega_n} \tag{26}$$

where $T_{\text{settling}} = 15$ s and the real part of the dominant closed-loop poles is $2p_1 = -\zeta\omega_n \approx -0.3$. Parameter $p_2 = -100$ was selected to be arbitrarily large ($\gg$ control bandwidth).

The results of the design are summarized in Table 3. All of the controllers are stable and minimum phase. They all resemble a triple lead network with ample gain/phase margin as expected from classical design point of view (see root locus plots and Bode plots of each design). The controller transfer functions are listed in the Appendix.

Typical sensor noise can be modeled as a small magnitude sinusoidal signal at a frequency that is much higher than the control bandwidth. For all three designs, the sensor noise is modeled as

$$v(t) = 0.001 \sin(100t) \tag{27}$$

A. Design 1

In this design, an extra weighting was employed to penalize the control signal u_2 in addition to the penalty on the spring constant $(u_1 - y_1)$. The purpose is to minimize the control energy to some extent without introducing conservativeness. The cost function has now become

$$\min_{F(s)} \left\| \begin{bmatrix} \gamma_1 T_{y_1 u_1} \\ \rho T_{u_2 u_1} \end{bmatrix} \right\|_\infty < 1 \tag{28}$$

Two types of controller were examined in this design, minimum phase and nonminimum phase. They both can be obtained by adjusting the bilinear transform parameters p_1 and p_2. The objective here is to maximum the robustness level γ with minimum control energy $1/\rho$. Two tradeoff curves that bound the stabilizing controllers are shown in Fig. 5 for two different settling time requirements (15 and 20 s). As control energy gets larger and larger, the robustness level increases.

Table 2 Design parameters

Design	p_1	p_2
1a	−0.35	−100
1b	−0.30	∞
2	−0.35	−100
3	−0.30	−100

Table 3 Design results

Design	Robustness	Settling time	Gain/phase margin
1a	$\|T\|_\infty < 1$	Figure 6 $T_s \approx 15$ s	18 < GM < 27 (dB) 68 < PM < 70 (deg)
1b	$\|T\|_\infty < 1$	Figure 12 $T_s \approx 15$ s	1.5 < GM < 4 (dB) 3 < PM < 30 (deg)
2	Figure 10b $\Delta \approx \pm 28\%$	Figure 12 $T_s \approx 15$ s	14 < GM < 21 (dB) 55 < PM < 68 (deg)
3	$\|T\|_\infty < 1$	Figures 14 $T_s \approx 20$ s	14 < GM < 20 (dB) 28 < PM < 53 (deg)

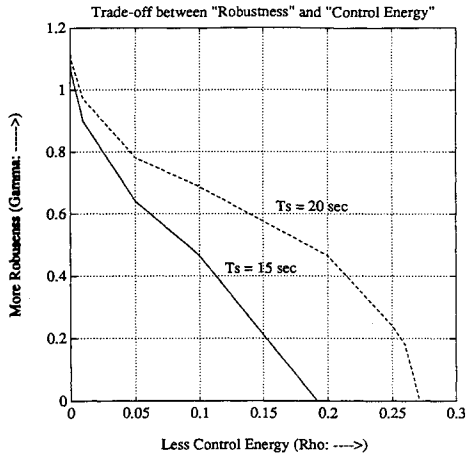

Fig. 5 Tradeoff curves for robustness and control energy.

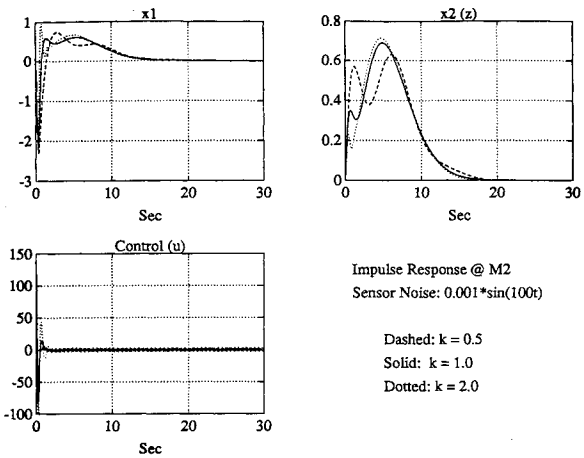

Fig. 6 Design 1a impulse response at mass 2.

Minimum Phase Controller (Design 1a)

Figures 6 and 7 show a design with robustness level $\gamma = 0.75$ and control energy constraint $\rho = 0.02$. Figure 6 shows the response of unit-impulse disturbance applied at mass 2. Clearly, mass 2 settling time meets the specification and the system is robust against spring constant variations ($0.5 < k < 2$) as well as high-frequency sensor noise. Figure 7 shows the controller Bode plot, overall loop transfer function, and root locus. As indicated, this design also enjoys large gain and phase margins. The root locus of the system indicates that the system is effectively controlled by a three-lead H^∞ controller with dominant closed-loop poles placed at desired locations (marked as boxes in Fig. 7).

Caveat. Since we bounded the uncertainty inside a complex disk with radius 0.75 ($\gamma = 0.75$), the control energy shown in Fig. 6 can be substantially reduced, when a real design tool is used to deal with real parametric variations.[15]

Nonminimum Phase Controller (Design 1b)

As an alternative design, a nonminimum phase type controller was also investigated. Simply because a minus sign in such a controller contributes 180-deg phase compensation with minimum control effort.

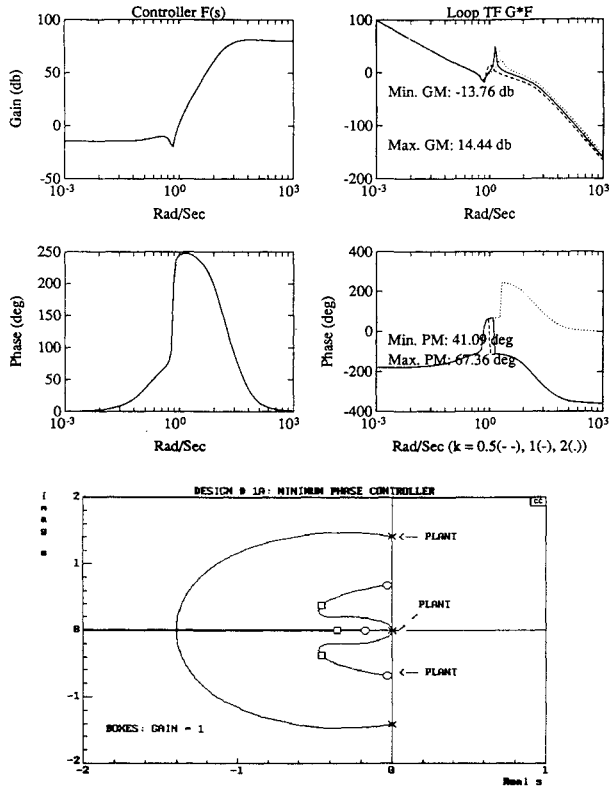

Fig. 7 Bode plots of H^∞ controller, loop transfer function, and root locus (design 1a).

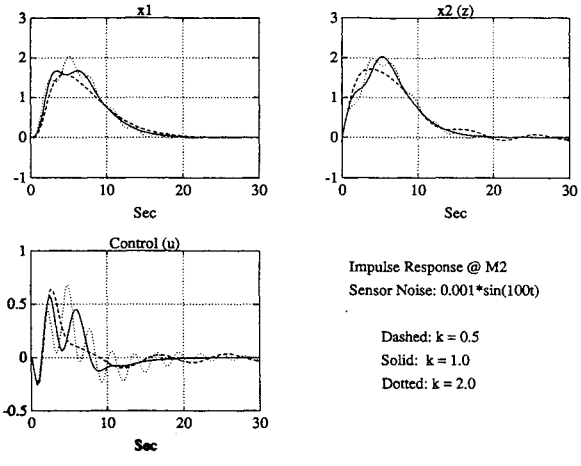

Fig. 8 Design 1b impulse response at mass 2.

Figures 8 and 9 show a design with robustness level $\gamma = 0$ and control energy constraint $\rho = 0.01$. The bilinear transform parameters were chosen to be $p_1 = -0.3$ and $p_2 = \infty$ to ensure a strictly proper controller with minimum high-frequency noise amplification. Figure 8 shows the impulse response at mass 2. Clearly, the mass 2 settling time meets the specification and the system is robust against spring constant variations ($0.5 < k < 2$) as well as high-frequency sensor noise. Figure 9 shows the controller Bode plot, overall loop transfer function, and root locus.

Caveat. As shown in Fig. 8, the control energy has been reduced substantially, but unfortunately, so have the gain and phase margins as compared to design 1a.

B. Design 2

For this design, the main requirement is to maximize the multivariable stability margin (MSM) for simultaneous (M_1, M_2, k) variations. This problem falls naturally into the framework of μ synthesis.[14]

First, a direct H^∞ design was formulated with additive uncertainties of M_1, M_2, and k pulled out and penalized as an H^∞ small-gain problem. Then following the usual μ synthesis procedure, an optimal H^∞ controller $F(s)$ is found so as to minimize $\|T_{y_1u_1}\|_\infty$. The optimal γ is $\gamma = 0.017$. The structured singular value routine[3] is then used to compute the MSM of $\gamma T_{y_1u_1}$ as well as the 3×3 diagonal scaling matrix $D(j\omega) = \text{diag}[d_1(j\omega), d_2(j\omega), d_3(j\omega)]$ (see Figs. 10a and 11a). The next step is to curve fit the magnitude Bode plots of diagonal scalings of $|d_1(j\omega)|$, $|d_2(j\omega)|$, $|d_3(j\omega)|$ with low-order stable and minimum-phase transfer functions and then absorb them into the plant $P(s)$ for another H^∞ design iteration (see Figs. 11b–d for the curve fitting). This procedure, which is repeated iteratively, first solving for $F(s)$ then $D(s)$, is called the *D-F* iteration.

We stopped after only one *D-F* iteration, since the size of the resulting controller has already increased from 4 states to

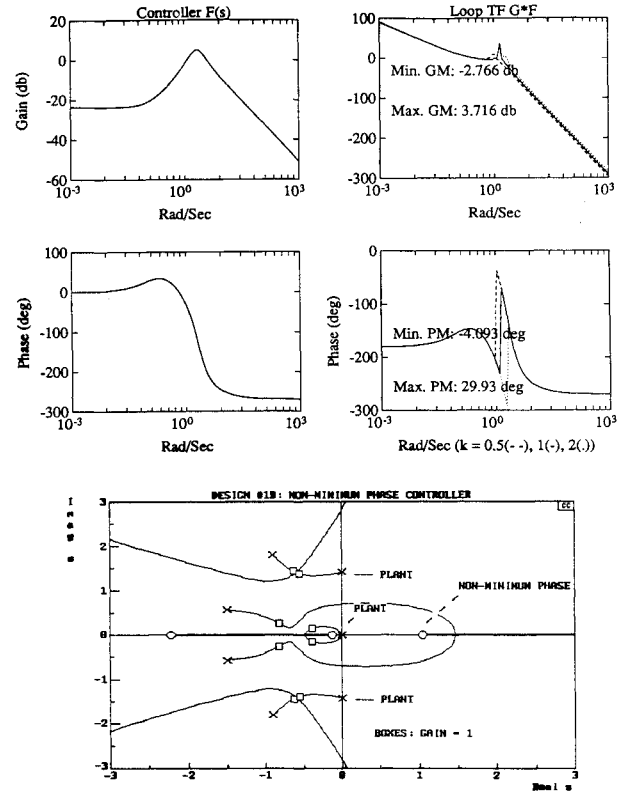

Fig. 9 Bode plots of H^∞ controller, loop transfer function, and root locus (design 1b).

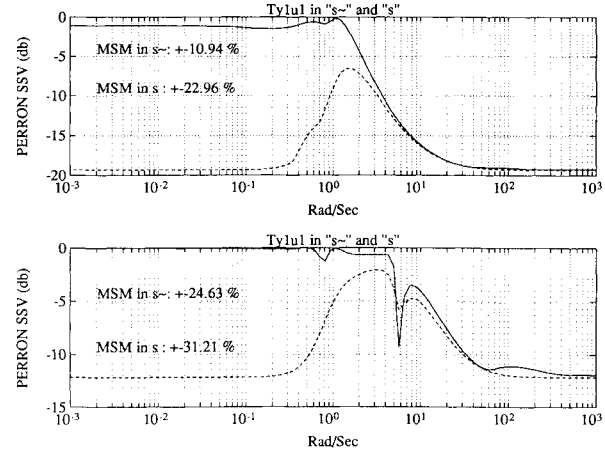

Fig. 10 Design 2: structured singular values.

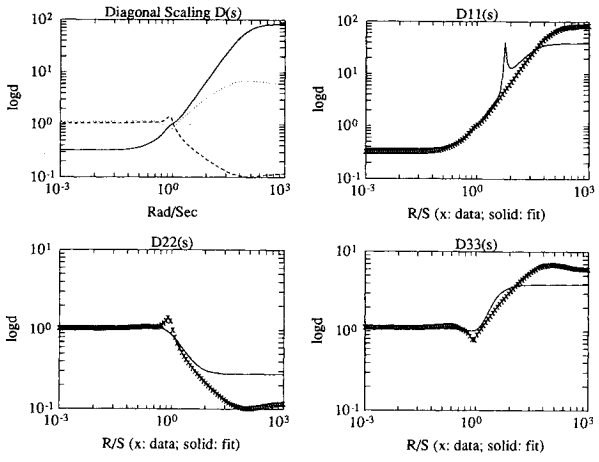

Fig. 11 Design 2: diagonal scaling $D(s)$ and curve fitting.

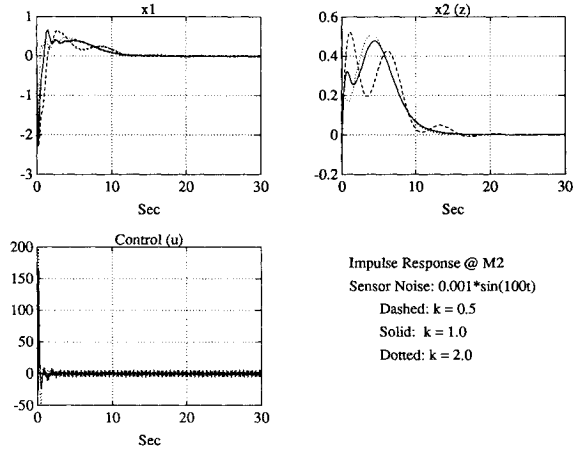

Fig. 12 Design 2 impulse response at mass 2.

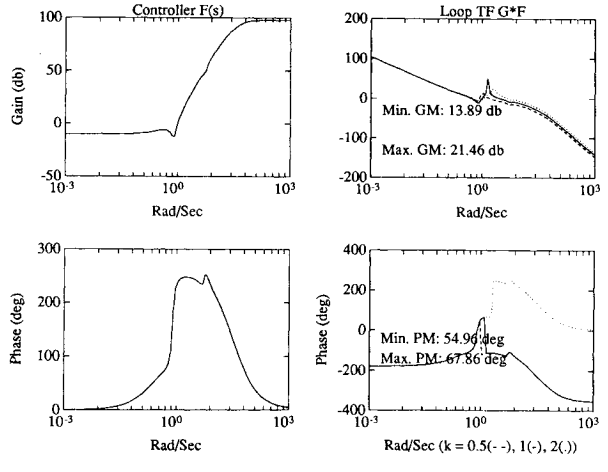

Fig. 13 Bode plots of H^∞ controller and loop transfer function.

16 states. The optimal γ increased to $\gamma = 0.17$. The resulting structured singular value plot is shown in Fig. 11b. The final MSM is improved by 12%.

Figure 12 shows the impulse response at mass 2. The settling time specification of mass 2 is met. The system is robust against $\pm 31\%$ simultaneous complex plant variations in (M_1, M_2, k) as well as high-frequency sensor noise. Figure 13 shows the controller Bode plot and the overall loop transfer function. Like design 1, this design also enjoys large gain and phase margins.

Caveat. Since we used the complex μ synthesis tool to design a controller for the real parametric variations, the control energy shown in Fig. 12 can be substantially reduced when a better tool is developed to deal with the real uncertainties.[15]

C. Design 3

In this design, a persistent sinusoidal disturbance [$\omega(t) = \sin(0.5t)$] is acting on the plant instead of the impulse disturbance. The basic requirements are still the same except the settling time of mass 2 has been relaxed to 20 s.

The internal model principle[12] indicates that to reject such a plant disturbance one can simply augment the plant at its control input with a compensator having poles coinciding with the disturbance poles, i.e., $s = \pm 0.5j$, then design an H^∞ controller for the augmented plant. In our design, the plant was compensated as follows,

$$G(s) \leftarrow G(s)\frac{(s+\alpha)^2}{s^2+\omega^2} \tag{29}$$

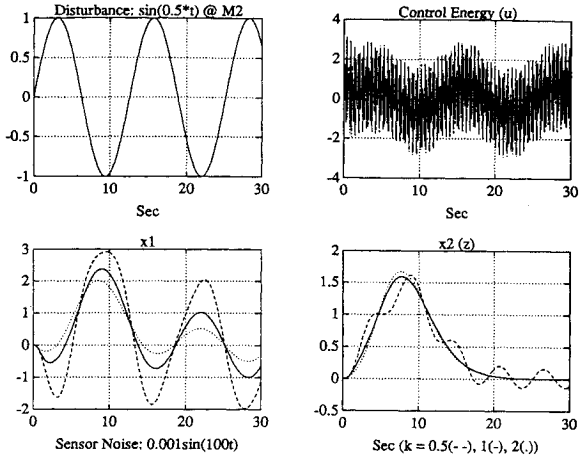

Fig. 14 Design 3: response of sinusoidal disturbance at mass 2.

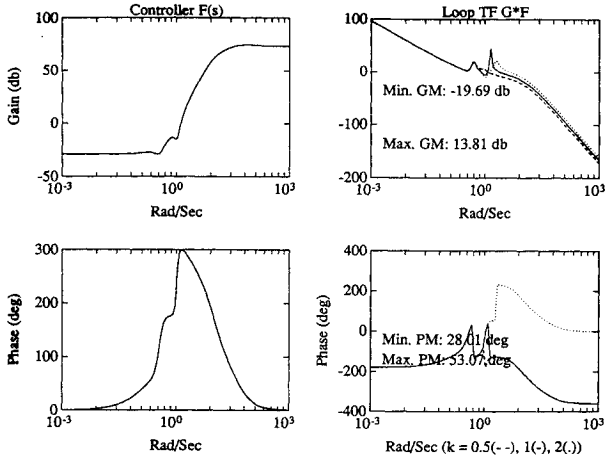

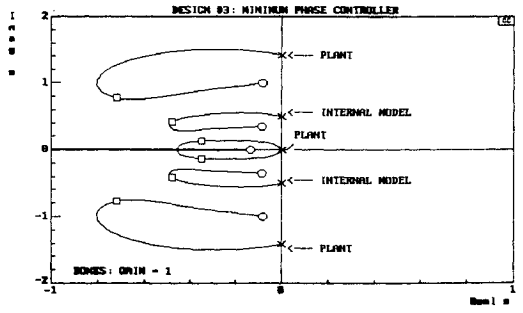

Fig. 15 Bode plots of H^∞ controller, loop transfer function, and root locus (design 3).

where $\alpha = 1 (>$ control bandwidth) to provide enough damping and $\omega = 0.5$, the disturbance frequency.

Figures 14 and 15 show a design with $\gamma = 0.4$ and $\rho = 0.01$. Figure 14 clearly indicates that settling time of mass 2 is exactly 20 s, and the system is robust against spring constant variations ($0.5 < k < 2$) as well as high-frequency sensor noise. Figure 15 shows the controller Bode plot and overall loop transfer function. Similar to designs 1 and 2, this design also enjoys large gain and phase margins. Figure 15 shows root locus of the system, which indicates that the system is effectively controlled by a five-lead minimum phase H^∞ controller with dominant closed-loop poles placed at desired locations (marked as boxes in Fig. 15).

Caveat. Since we bounded the uncertainty inside a complex disk with radius 0.4 ($\gamma = 0.4$), the control energy shown in Fig. 14 may be reduced a bit more using a real μ design tool.[15]

Remark. A MATLAB demo of these three design problems can be found in Ver. 2.0 of the *Robust-Control Toolbox*[3] released in Aug. 1992.

IV. Conclusions

A four-state stable, minimum-phase H^∞ controller has been found for each of the three benchmark design problems. A simple bilinear transform is found to be extremely useful in designing the H^∞ robust controller to meet the settling time specification since it enables one to place closed-loop poles of the H^∞ control system inside a disk-shaped region. The tools we used have treated the real uncertainties as complex, which may be the only caveat in the whole approach. A better tool that can deal with mixed real and complex uncertainties is under development.[15] All of the design specifications have been satisfied.

Appendix: Controller Transfer Functions

Design 1a

$$F(s) = \frac{10084(s + 100)(s + 0.17285)[(s + 0.03135)^2 + 0.6759^2]}{[(s + 50.494)^2 + 2.6838^2][(s + 9.7294)^2 + 8.2677^2]} \tag{A1}$$

Design 1b

$$F(s) = \frac{2.5622(1.043 - s)(s + 2.2168)(s + 0.1221)}{[(s + 0.9072)^2 + 1.8114^2][(s + 1.4945)^2 + 0.578^2]} \tag{A2}$$

Design 2 (after model reduction)

$$F(s) = \frac{46978(s + 0.22)(s + 99.89)[(s + 0.58)^2 + 5.53^2][(s + 0.067)^2 + 0.78^2]}{[(s + 1.029)^2 + 5.76^2][(s + 21.8)^2 + 8.21^2][(s + 53.4)^2 + 7.13^2]} \tag{A3}$$

Design 3 (internal model included):

$$F(s) = \frac{4642.4(s + 0.134)(s + 100)[(s + 0.0843)^2 + 0.3508^2][(s + 0.08378)^2 + 1.0212^2]}{(s^2 + 0.5^2)[(s + 6.8989)^2 + 6.8764^2][(s + 50.276)^2 + 1.721^2)]} \tag{A4}$$

Acknowledgment

This work was supported in part by Air Force Office of Scientific Research Grant F49620-92-J-0014.

References

[1]Wie, B., and Bernstein, D. S., "A Benchmark Problem for Robust Control Design," *Proceedings of the American Control Conference* (San Diego, CA), Inst. of Electrical and Electronics Engineers, New York, 1990, pp. 961-962.

[2]Safonov, M. G., "Imaginary-Axis Zeros in Multivariable H^∞ Optimal Control," *Modeling Robustness and Sensitivity Reduction in Control Systems,* edited by R. F. Curtain, Springer-Verlag, New York, 1987, pp. 70-81.

[3]Chiang, R. Y., and Safonov, M. G., *Robust-Control Toolbox,* MathWorks, Natick, MA, 1988.

[4]Chiang, R. Y., "Modern Robust Control Theory," Ph.D. Dissertation, Dept. of Electrical Engineering, Univ. of Southern California, Los Angeles, CA, Dec. 1988.

[5]Mageriou, E. F., and Ho, Y. C., "Decentralized Stabilization via Game Theoretic Methods," *Automatica,* Vol. 13, No. 4, 1977, pp. 393-399.

[6]Khargonekar, P. P., Petersen, I. R., and Rotea, M. A., "H^∞ Optimal Control with State Feedback," *IEEE Transactions on Automatic Control,* Vol. AC-33, No. 8, 1988, pp. 783-786.

[7]Doyle, J. C., Glover, K., Khargonekar, P., and Francis, B., "State-Space Solutions to Standard H^2 and H^∞ Control Problems," *IEEE Transactions on Automatic Control,* Vol. AC-34, No. 8, 1989, pp. 831-847.

[8]Limebeer, D. J. N., Kasenally, E. M., Jaimouka, E., and Safonov, M. G., "A Characterization of all Solutions to the Four Block General Distance Problem," *Proceedings of the 27th IEEE Conference on Decision and Control,* Inst. of Electrical and Electronics Engineers, New York, 1988, pp. 875-880.

[9]Safonov, M. G., Limebeer, D. J. N., and Chiang, R. Y., "Simplifying the H^∞ Theory via Loop Shifting, Matrix Pencil and Descriptor Concepts," *International Journal of Control,* Vol. 50, No. 6, 1989, pp. 2467-2488.

[10]Chiang, R. Y., Safonov, M. G., and Tekawy, J. A., "H^∞ Flight Control Design with Large Parametric Robustness," *Proceedings of the American Control Conference* (San Diego, CA), Inst. of Electrical and Electronic Engineers, New York, 1990, pp. 2496-2501.

[11]Dorf, R., *Modern Control Systems,* 5th ed., Addison-Wesley, Reading, MA, 1989.

[12]Francis, B., and Wonham, W. M., "The Internal Model Principle for Linear Multivariable Regulators," *Applied Mathematics and Optimization,* Vol. 2, No. 2, 1975, pp. 170-194.

[13]Safonov, M. G., and Chiang, R. Y., "CACSD Using the State-Space L^∞ Theory—A Design Example," *IEEE Transactions on Automatic Control,* Vol. AC-33, No. 5, 1988, pp. 477-479.

[14]Safonov, M. G., "L^∞ Optimal Sensitivity vs. Stability Margin," *Proceedings of the 22nd IEEE Conference on Decision and Control,* Inst. of Electrical and Electronics Engineers, New York, 1983, pp. 115-118.

[15]Chiang, R. Y., and Safonov, M. G., "Real Km-Synthesis via Generalized Popov Multipliers," *Proceedings of the 1992 American Control Conference,* Inst. of Electrical and Electronic Engineers, New York, 1992, pp. 2417-2418.